Correlation between DSC Curves and Isobaric State Diagrams. 2. Concentration-Dependence of Eutectic Peak Widths in DSC Curves

Andreas Müller and Werner Borchard*

Angewandte Physikalische Chemie, Gerhard-Mercator-Universität Duisburg, Lotharstrasse 1, D-47048 Duisburg, Germany

Received: November 13, 1996; In Final Form: March 4, 1997[⊗]

The concentration-dependence of the eutectic peak widths in isobaric DSC curves is investigated. Pursuant to the relationships derived, these widths become maximum at the eutectic point. Depending on the thermophysical properties of the sample, further maxima might arise of which the loci are predictable. The correlation between the heat flow registered during a DSC scan and the specific heat capacity represented in the DSC curve is met under certain conditions only. A precise determination of heat capacities by DSC is thus questionable.

1. Introduction

Transitions of the first order according to Ehrenfest's relations reveal a steplike change in enthalpy at their transition point.[1] Their derivative, the $\tilde{c}_P(T)$ curve, is thus also discontinuous at this point due to an infinitely sharp and high peak. That is, the specific heat capacity of a sharply melting substance, such as a pure compound or a eutectic (mixture), is not defined at its melting point in terms of thermodynamics.

Owing to a limited isobaric heat flow $\dot{Q}$ in dynamic calorimeters, such as the differential scanning calorimeter (DSC),

$$\dot{Q} = (\partial Q/\partial t)_P \qquad (1)$$

understood to be the change of heat Q per unit time, the experimental peaks will, however, not be infinitely sharp, as anticipated in thermodynamic terms, but represent those being more or less broadened to a range of fusion of a certain extent. This time delay of a thermal event due to heat conduction processes leading to a peak broadening is customarily called "smearing".[2] Since $\tilde{c}_P(T)$ curves of real DSC scans are inevitably subject to smearing, transition peaks obtainded by DSC are always "defined" at their transition points with respect to the heat capacity. Accordingly, their transition enthalpy can be assigned to the peak area by use of eq 1 after integration over the entire range of transition. However, it must be observed that heat does not constitute a state function being invariant to the pathway of process on which the final state has been reached. To denote inexact differentials in contrast to the total differentials of state functions, the differential sign of the former is usually provided with a bar across it (đ). As, however, the heat exchanged under isobaric conditions is equivalent to the change of enthalpy, we shall refrain from a particular indication of the differential signs.

In the last paper,[3] we have dealt with the calculation of "ideal" (i.e. nonsmeared) $\tilde{c}_P(T)$ traces of DSC curves from a known isobaric phase diagram, using *n*-hexane and *n*-dodecane as model compounds. Since this binary model system is of the eutectic type, a Gaussian distribution has been taken as a basis to render the calculated—and infinitely sharp—eutectic fusion peaks representable. Their widths have thereby been related to those of the pure components of the underlying system. However, the experimental eutectic peaks turned out to be only poorly reproduced because the intial concentration, w_2°, exerts a dominant influence on their widths. The goal of the present paper is therefore to investigate the concentration-dependence of the eutectic peak widths in DSC curves. Insofar as different masses of the samples might disturb the accuracy of our investigations with regard to the eutectic peak widths, the underlying binary model system chosen was *n*-eicosane (n-$C_{20}H_{42}$)/*n*-triacontane (n-$C_{30}H_{62}$), of which the samples were to be as similar in mass as possible. The isobaric state diagram thereof is drawn in Figure 1.

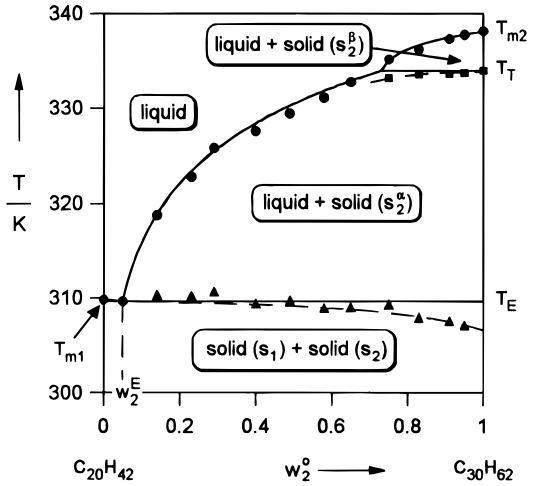

Figure 1. Isobaric eutectic state diagram of the underlying binary model system n-$C_{20}H_{42}$/n-$C_{30}H_{62}$ depicting the liquidus temperatures (●), the eutectic temperatures (▲), and the temperatures of an incongruently melting (■) of *n*-triacontane as a function of the overall composition w_2° of the sample given in the mass fraction scale (see text).

2. Phenomenological Thermodynamic Considerations

In the following, we adopt an admittedly oversimplified picture of eutectic crystallization. For instance, the rates of cooling are conveniently assumed to be so small that the system has been allowed to establish all possible equilibria by diffusion.

* To whom correspondence should be addressed.

[⊗] Abstract published in *Advance ACS Abstracts,* April 15, 1997.

S1089-5647(96)03782-0 CCC: $14.00

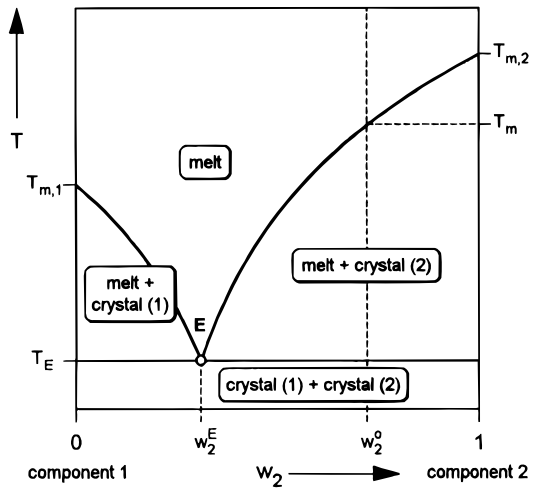

Figure 2. Schematic plot of an isobaric eutectic state diagram showing temperature T as a function of the mass fraction w_2. $T_{m,1}$ and $T_{m,2}$: melting temperatures of the pure component 1 and 2, respectively. T_m: melting temperature of the binary test sample. **E**: invariant eutectic point at the eutectic temperature, T_E, and at the eutectic composition, w_2^E; w_2^o: total or initial composition of the sample to be investigated.

In other words, the relative amounts of the coexisting phases are taken during crystallization as being changed following the lever rule. According to the schematic plot of a eutectic phase diagram shown in Figure 2, cooling a homogeneous liquid mixture consisting of component 1 and component 2 with an initial composition w_2^o results in a phase separation, actually into the binary melt and the pure crystal 2, after passing the liquidus curve and entering the two-phase region at temperature T_m (being the temperature of crystallization or fusion of the binary sample). On approaching the eutectic temperature T_E, the remaining liquid phase, which corresponds to the binary eutectic mixture, settles down in the gravitational field to give the binary eutectic crystal. During this cooling procedure the liquid eutectic mixture should—under the above-assumed "ideal" cooling conditions—crystallize on top of the pure crystal 2 that has been precipitated before (see Figure 3a). Application of O'Neill's model for sharply melting pure compounds[4] to the invariant eutectic transition will thus require an additional (inert) layer of the pure crystal 2 to be taken into account.

Throughout the next section (section 2.1) we shall be dealing with the widths of the eutectic fusion peaks in DSC curves, which are understood to be the distances between the foot points of the peak onset and the peak end. In particular, we shall look at the fusion process at different stages of time and simplify the following treatise on heat conduction by introducing steady-state conditions. Subsequently in section 2.2, we shall then turn to a discussion of the concentration-dependence of the eutectic peak widhts. To this end, the relationships derived will be reduced to experimentally accessible quantities. Finally, the correlation between the heat flow recorded in the course of the eutectic transition and the specific heat capacity will be given.

2.1. Quantitative Description of Eutectic Peak Widths. The DSC apparatus utilized is considered to consist of a platform P (sample-holder) denoted by the lowest segment (Figure 3a), which is connected to the temperature source S generating the program temperature T_P. Our sample, assumed to be initially composed of two stacked homogeneous and isotropic layers, namely, the pure crystal 2 and the eutectic mixture designated by the segment S_I and S_{III} in Figure 3a, is enclosed by an aluminum-pan (sample-container), which in turn rests on the sample-holder. On running a DSC scan the current temperature T_P of source S will be increased with time t by the constant heating rate, $\dot{T}_P$, under isobaric conditions:

$$\dot{T}_P = (\partial T_P/\partial t)_P \tag{2}$$

Starting out at time $t = 0$ when temperature $T_P(z_P)$ of source S equals the eutectic temperature, T_E, the two lowest layers, namely, platform P and segment S_I with the pure component 2, have to be traversed by the heat Q supplied one-dimensionally to the system, to enhance temperature $T_I(z_I)$ to T_E. Due to the thermal resistances R_0 and R_I on the route through the two lowest segments P and S_I, a time-delayed heat transfer is observed. In other words, if the sample-holder has reached the eutectic temperature, T_E, it will take a certain time t_0 until $T_I(z_I)$ matches T_E (Figure 3a). At this time, an additional layer of the melted eutectic appears at z_I (segment S_{II}). Its upper boundary, a solid—liquid interface, $z_{II} = f(t)$, starts moving up through the sample toward the upper surface z_{III} of segment S_{III} since the heat Q released to the aluminum-pan at z_0 is completely absorbed at this interface, which brings about a partial fusion of the eutectic crystal. This very moment constitutes the onset of the eutectic transition. We may therefore take $z_I = 0$ at $T_I = T_E$ and $t = t_0$ as a relative zero of motion of the aforementioned interface; hence, the thickness of this additional layer, Δz_{II}, which will be defined below (see eq 6) equals 0 at this time ($\Delta z_{II}(t_0) = 0$).

(Strictly speaking, there is no heat released to the calorimeter, but in effect, electrical heating power is performed at temperature source S to establish the program temperature T_P at time t. Apart from negligible "losses of energy" in the system incurred due to the electrical resistance of the heating element of source S, the electrical work may be conceived to be completely transformed into heat exchanged subsequently with the sample at the lowest plane z_P. Consequently, we shall not make any distinction between the electrical work done and the generated (one-dimensional) heat inflow $\dot{Q}$ being equivalent to the heat input supplied to the system per unit time.[5])

However, it should be emphasized here that one must not confuse the start of the DSC scan and the time $t = 0$. At the very beginning of a DSC measurement the total system to be investigated, i.e. the sample and the aluminum-pan as well, is in thermal equilibrium with the surroundings whose temperature is T_{III}. The time $t = 0$ is assigned to the moment at which the program temperature T_P of platform P has reached the eutectic transition temperature T_E. Time $t = t_0$, in turn, is the period of time for raising temperature T_I to T_E and corresponds to the onset of eutectic transition of fusion.

According to Fourier's first law, the heat flow $\dot{Q}$ in a one-dimensional system (z-direction) is determined by[6−9]

$$\dot{Q} = -A\lambda\left(\frac{\partial T}{\partial z}\right)_P \tag{3}$$

This empirical relationship of heat conduction characterizes the flow of heat in direction of z penetrating the cross-sectional area A of the uniform thermal conductor perpendicularly to the direction of the decreasing temperature, i.e. the negative isobaric temperature gradient, $-(\partial T/\partial z)_P$, which is the cause of the heat flow ("driving force"). The negative sign in eq 3 indicates that the heat flow is in the direction of the negative temperature gradient and serves to render $\dot{Q}$ positive. The constant of proportionality, λ, is termed the coefficient of thermal conductivity and is observed experimentally to depend on the thermophysical properties of the material through which the heat flows. It is worth noting that the thermal conductivity λ is not necessarily a constant but, in fact, is a function of temperature. For small, select temperature ranges, however, such as the fusion range of the eutectic transition, λ may be understood to be the

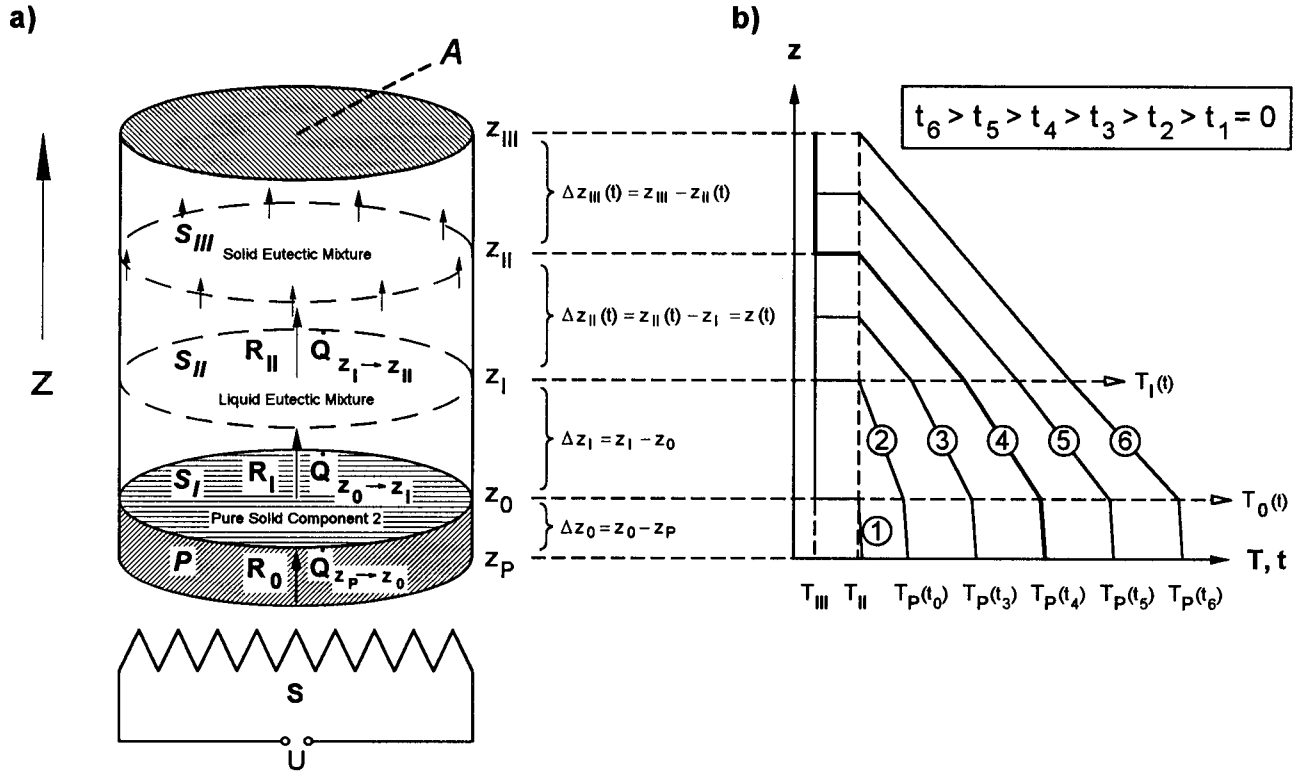

Figure 3. Diagram depicting sample geometry, linear heat flow (a), and temperature field (b) within the sample-container during a eutectic transition of fusion (see text). For the sake of clarity the sample-holder ***P*** additionally comprises the bottom of the sample-container.

mean value of this temperature interval. In the end, λ may also vary in direction unless the thermal conductor is anisotropic.

By imposing a linear course of temperature in each segment, application of eq 3 to the individual segments P, S_I, and S_{II} in Figure 3a yields

$$\dot{Q}_{z_P \to z_0} = -\frac{\Delta T_0}{\Delta z_0} A^* \lambda_0 = -\frac{\Delta T_0}{R_0} \tag{4a}$$

$$\dot{Q}_{z_0 \to z_1} = -\frac{\Delta T_I(t)}{\Delta z_1} A \lambda_I = -\frac{\Delta T_I(t)}{R_I} \tag{4b}$$

$$\dot{Q}_{z_I \to z_{II}} = -\frac{\Delta T_{II}(t)}{\Delta z_{1I}(t)} A \lambda_{II} = -\frac{\Delta T_{II}(t)}{R_{II}(t)} \tag{4c}$$

Here, the arrow in the index of $\dot{Q}$ indicates the heat flow from the lower bound z_i to the upper bound z_j of the segment in question;

$$\Delta T_0 = T_0 - T_P, \quad \Delta T_I(t) = T_I(t) - T_0, \quad \Delta T_{II}(t) = T_{II} - T_I(t) \tag{5}$$

are the temperature differences between the upper and the lower boundary of the layers involved, whose thicknesses are

$$\Delta z_0 = z_0 - z_P, \quad \Delta z_I = z_I - z_0, \quad \Delta z_{II}(t) = z_{II}(t) - z_I \tag{6}$$

and whose corresponding thermal resistances are

$$R_0 = \frac{\Delta z_0}{A^* \lambda_0}, \quad R_I = \frac{\Delta z_I}{A \lambda_I}, \quad R_{II}(t) = \frac{\Delta z_{II}(t)}{A \lambda_{II}} \tag{7}$$

where λ_0, λ_I, and λ_{II} designate the respective thermal conductivities. Area A of platform P has additionally been indicated by an asterisk (*) in order to draw a distinction between the former and those of the upper segments, due to the fact that indeed $A^* > A$. Furthermore, since P is also considered to comprise the bottom of the aluminum-pan, the exact geometry of the lowest segment is not known anyway.

It should be noted here that the replacement of the temperature gradients by temperature differences necessitates a steady-state conduction. In other words, a linear temperature field in each layer requires interfaces to be maintained at constant temperatures T_P, T_0, T_I, and T_E ($T_P > T_0 > T_I > T_E$) that will inevitably lead to a steady heat flow $\dot{Q}$ being invariant with respect to time:

$$\dot{Q} \equiv \dot{Q}_{z_P \to z_0} = \dot{Q}_{z_0 \to z_1} = \dot{Q}_{z_I \to z_{II}} \tag{8}$$

Equation 8 is the exact analogue to Kirchhoff's second law for an electrical conductor and describes the total heat flow $\dot{Q}$ passing the aforementioned segments in series, actually from the lowest boundary, z_P, to the solid−liquid interface at z_{II}. Accordingly, the corresponding thermal resistances connected in series are therefore given by the relation

$$R = R_0 + R_I + R_{II} = -\frac{\Delta T_0}{\dot{Q}_{z_P \to z_0}} - \frac{\Delta T_I}{\dot{Q}_{z_0 \to z_I}} - \frac{\Delta T_{II}}{\dot{Q}_{z_I \to z_{II}}} \equiv -\frac{\Delta T}{\dot{Q}} \tag{9}$$

established from eqs 4−8 by eliminating the intermediate temperatures T_0 and T_I. Clearly, the individual thermal resistances add up to a total resistance, R, which is related to the total thickness of the traversed layers, $\Delta z_0 + \Delta z_I + \Delta z_{II}$, and the total temperature difference, $\Delta T = T_E - T_P$. Since

$$T_P(t) = T_E + \dot{T}_P t \tag{10}$$

which proceeds from integrating eq 2 within the limits T_E ($t = 0$) and T_P ($t = t$), ΔT may also be expressed by the identity

$$\Delta T = T_E - T_P = -\dot{T}_P t \tag{11}$$

In reality, however, it is more heat supplied per time to the sample than absorbed at the same time at its upper surface z_{II} since T_P at source S is constantly rising with time and the temperatures at the internal planes, T_0 and T_I, do not remain constant either. Consequently, a time-dependent temperature profile in the direction of z is formed (see Figure 3b) that is contradictory to a steady flow $\dot{Q}$ being independent of time. Note that linear temperature profiles have been depicted schematically in Figure 3b at different times t although they should actually reveal a nonlinear course due to the permanent temperature rise at source S.

Courses 2 and 6 in Figure 3b denote the onset ($t = t_0$) and the end ($t = t_6$) of the eutectic transition, respectively, whereby in the latter case the melting front $z_{II}(t)$ has arrived at the upper boundary of segment S_{III} at z_{III}. In the event of 4 the bold line characterizes the relevant temperature field of the idealized picture of eutectic fusion at time t, as assumed in Figure 3a. Clearly, the temperature in the three lowest segments will not evenly be changed per time owing to the different thermal conductivities of the individual layers (whereby $R_0 < R_I < R_{II}$). For instance, as a consequence of the poor heat conductive properties of the pure solid 2 in segment S_I that corresponds to triacontane (n-$C_{30}H_{62}$) in the present case, temperature T_I at interface z_I is not increased with $\dot{T}_P$ but with the increment $\dot{T}_I$ instead:

$$\dot{T}_I = (\partial T_I/\partial t)_P \leq \dot{T}_P \tag{11a}$$

Equation 11a defines the effective heating rate at z_I being smaller in fact than the preset rate $\dot{T}_P$ of source S. At the same time the metallic platform P represents a very good thermal conductor, leading to an increment $\dot{T}_0$ that should equal $\dot{T}_P$:

$$\dot{T}_0 = (\partial T_0/\partial t)_P \approx \dot{T}_P \tag{11b}$$

In contrast, temperature T_{II} of the moving interface z_{II} does not change at all; it remains constant at the eutectic temperature T_E throughout the eutectic transition (i.e. $\dot{T}_{II} = 0$) because fusion always occurs isothermally.

(As a result of the different increments, namely, $\dot{T}_P \approx \dot{T}_0 > \dot{T}_I > \dot{T}_{II}$, the temperature field and the temperature differences of the layers are more or less time-dependent. Difference ΔT_0 of platform P is approximately invariant with respect to time so that the corresponding flow of heat $\dot{Q}_{z_P \to z_0}$ remains unchanged (due to $\dot{T}_P \approx \dot{T}_0$). Owing to $\dot{T}_0 > \dot{T}_I$, the temperature difference ΔT_I of layer S_I increases marginally and hence $\dot{Q}_{z_0 \to z_I}$ as well. Since temperature T_{II} is constant during the eutectic transition while T_I rises continually with time, the temperature difference of the melted eutectic, ΔT_{II}, grows noticeably. Simultaneously, the layer thickness $\Delta z_{II}(t)$ and therefore the thermal resistance $R_{II}(t)$ of this layer are increasing quantities. This brings about a flow of heat $\dot{Q}_{z_I \to z_{II}}$, which may be assumed not to be influenced by time. For this reason, a steady heat conduction pursuant to eq 8 can safely be accepted as a satisfactory approximation.)

The heat flow at the solid−liquid interface $z_{II}(t)$ is taken to be only determined by the rate at which the eutectic melts, which is proportional to the interface velocity:[4]

$$\dot{Q} = \left(\frac{\partial H_{II}}{\partial t}\right)_P = \left(\frac{\partial H_{II}}{\partial z}\right)_P \left(\frac{\partial z}{\partial t}\right)_P \tag{12}$$

Here, z denotes the interface $z_{II}(t)$ or rather the present layer thickness $\Delta z_{II}(t)$ of segment S_{II}, since the motion of this interface has been related to a relative zero at $z_I = 0$ and $t = t_0$:

$$z(t) \equiv \Delta z_{II}(t) = z_{II}(t) \tag{13}$$

Consequently, the explicit designation of the moving interface and its corresponding layer thickness may be abandoned from now on. Examination of eq 12 shows clearly that the heat flow at this solid−liquid interface is equivalent to the isobaric change of enthalpy per time, $(\partial H_{II}/\partial t)_P$, which in turn may be taken as the product of $(\partial H_{II}/\partial z)_P$ and $(\partial z/\partial t)_P$. These two isobaric differential coefficients represent the change of enthalpy as a function of the growing layer thickness of segment S_{II} (part of the enthalpy gradient) and the corresponding interface velocity, respectively.

(It should be kept in mind, however, that eq 12 is based on the assumption that the heat flow released to the sample brings about the eutectic transition. This is synonymous with an isothermal transfer of a eutectic solid into the liquid state at temperature T_E. In reality, however, a minor flow is additionally necessary to raise the present temperature of the eutectic crystal, T_{III}, to the transition temperature, T_E, prior to the transition proper, but without being melted hereby. The heat flow is therefore identical with the enthalpy change of the eutectic crystal with time, which in turn is proportional to the total mass of the sample, m, to the specific heat capacity of this crystal, $\tilde{c}_{P_{III}}$, and to the local rate of temperature change, $\dot{T}_{III}$,

$$\dot{Q}_{z_{II}} = \left(\frac{\partial H_{III}}{\partial t}\right)_P = \left(\frac{\partial H_{III}}{\partial T_{III}}\right)_P \left(\frac{\partial T_{III}}{\partial t}\right)_P = m\tilde{c}_{P_{III}}\dot{T}_{III} \tag{14a}$$

Here, $\dot{T}_{III}$ only applies to the solid−liquid interface, z_{II}, so that the temperature in segment S_{III} remains constant. In addition, inasmuch as temperature T_P of the heat source S is evenly growing with $\dot{T}_P$ in the interim, a futher contribution of energy needs to be expended on establishing the temperature field at a certain time t, as depicted in Figure 3b. We may thus formulate this supplementary heat flow at any site z_x in the system (whereby $z_P \leq z_x < z_{II}$):

$$\dot{Q}_{z_x} = \left(\frac{\partial H}{\partial t}\right)_P = \left(\frac{\partial H}{\partial T}\right)_P \left(\frac{\partial T}{\partial t}\right)_P = m\tilde{c}_P\dot{T}_x \tag{14b}$$

where $\tilde{c}_P$ designates the specific heat capacity of the respective layer. Rate $\dot{T}_x$ introduced is the effective heating rate at z_x and must not be mistaken for the preset heating rate $\dot{T}_P$. Since, however, an enthalpy change caused by a temperature rise is orders of magnitudes smaller than that being subjected to melting, the flows $\dot{Q}_{z_{II}}$ and $\dot{Q}_{z_x}$ in eqs 14a and 14b are negligible with respect to the "proper" heat flow $\dot{Q}$ in eq 12). For this reason, we shall assume in the following that the flow absorbed is entirely used up by the eutectic enthalpy of fusion.)

Let $V_{II}(z)$ be the volume of segment S_{II} that is a function of its present layer thickness z(t),

$$V_{II}(z) = Az = m_{II}(z)/\rho_{II} \tag{15}$$

Solving eq 15 for z and incorporating the first derivative of z with respect to m_{II} in eq 12, eq 12 may be rewritten yielding

$$\dot{Q} = \left(\frac{\partial H_{II}}{\partial t}\right)_P = \left(\frac{\partial H_{II}}{\partial m_{II}}\right)_P A\rho_{II}\left(\frac{\partial z}{\partial t}\right)_P \tag{16}$$

where ρ_{II} is the density of the eutectic melt in segment S_{II}, and A the constant cross-sectional area of the sample that is also equivalent to the area of the moving solid−liquid interface z(t). In addition, the differential coefficient $(\partial H_{II}/\partial m_{II})_P$ corresponds to the changing eutectic enthalpy of fusion with respect to the mass $m_{II}(z)$. Hence an inifinitesimal amount of enthalpy, dH_{II},

must be expended to create a eutectic melt with a layer thickness dz whose mass is dm_{II}.

Regarding the total period of the eutectic transition, i.e. from time t_0 to the present time t, we may approximate

$$\left(\frac{\partial H_{II}}{\partial m_{II}}\right)_P \approx \frac{\Delta H_{II}}{m_{II}} \tag{17a}$$

corresponding to an average value of enthalpy change with mass m_{II}: ΔH_{II} is the eutectic enthalpy of fusion that needs to be expended to transfer a solid eutectic with the mass $m_{II}(z)$ into the liquid state, or simply to generate a eutectic melt with a layer thickness z(t). Since the specific eutectic enthalpy of fusion, $\Delta\tilde{H}_{II}$, is correlated with the total mass of the sample, m, which is given by the identity

$$m = m_I + m_{II} \tag{17b}$$

eq 17a can be rearranged

$$\frac{\Delta H_{II}}{m_{II}} = \frac{\Delta H_{II}}{m}\frac{m}{m_{II}} = \Delta\tilde{H}_{II}\left(1 + \frac{m_I}{m_{II}}\right) \tag{17c}$$

leading to

$$\dot{Q} = \left(1 + \frac{m_I}{m_{II}}\right)\Delta\tilde{H}_{II}A\rho_{II}\left(\frac{\partial z}{\partial t}\right)_P \tag{18}$$

Combination of eq 9 with eq 11 followed by substitution of $\dot{Q}$ by means of eq 18 affords

$$\dot{T}_P t\, dt = (R_0 + R_I + R_{II})\left(1 + \frac{m_I}{m_{II}}\right)\Delta\tilde{H}_{II}A\rho_{II}dz \tag{19}$$

By replacing R_{II}, defined by eq 7, into eq 19 and integrating within the period from t_0 (z = z_I = 0) to t (z) being identical with the elapsed time of eutectic fusion, we obtain

$$\frac{\dot{T}_P}{2}(t^2 - t_0^2) = \left(1 + \frac{m_I}{m_{II}}\right)\Delta\tilde{H}_{II}\left[A\rho_{II}(R_0 + R_I)z + \frac{\rho_{II}}{\lambda_{II}}\frac{z^2}{2}\right] \tag{20}$$

The present layer thickness z of segment S_{II} may be eliminated by incorporating eq 15 into eq 20. Solving for time t yields

$$t = \sqrt{\frac{\Delta\tilde{H}_{II}m}{\dot{T}_P}[2(R_0 + R_I) + R_{II}] + t_0^2} \tag{21a}$$

where

$$R_{II} = \frac{m_{II}}{A^2\lambda_{II}\rho_{II}} \tag{21b}$$

(see eq 7). This is the duration of the eutectic transition of fusion whereby a eutectic crystal with the mass m_{II} and the layer thickness z is transferred into the liquid state. Simplifying the foregoing relationships by equating the mass m_I to zero (so that $\Delta z_I = 0$, $R_I = 0$) and assuming $t_0 \rightarrow 0$ approximately would reduce eq 21 to an expression that may be shown to be equivalent to that derived originally by O'Neill for sharply melting substances.[4] If the layer S_I containing the crystalline component 2 did not exist, our model of a eutectic melting process, as shown in Figure 3, would hence turn into the fusion of a pure substance or, likewise, the fusion of a eutectic crystal at the eutectic point.

Since the eutectic transition commences at time t_0 and is terminated at $t_0 + t$, we are capable of introducing the definition of ΔT_E, the width of a eutectic fusion peak at its foot, by integrating eq 2 within these limits:

$$\Delta T_E = T_P(t + t_0) - T_P(t_0) = \dot{T}_P t \tag{22}$$

Incorporation into eq 21 furnishes the final expression

$$\Delta T_E = \sqrt{\Delta\tilde{H}_{II}m\dot{T}_P[2(R_0 + R_I) + R_{II}] + (\dot{T}_P t_0)^2} \tag{23}$$

2.2. Concentration-Dependence of Eutectic Peak Widths. With eq 23 at hand, we have at our disposal a means for calculating eutectic peak widths, ΔT_E, in isobaric DSC curves. It may also serve to investigate the concentration dependence of the eutectic peak widths because R_I, R_{II}, and $\Delta\tilde{H}_{II}$ depend on the initial concentration w_2°. Resistance R_I refers to the pure crystal of component 2 and is preferably written in experimentally accessible quantities,

$$R_I = m_I/(A^2\lambda_I\rho_I) \tag{24a}$$

which is due to elimination of thickness Δz_I in eq 7 by a relation equivalent to eq 15:

$$\Delta z_I = m_I/(\rho_I A) \tag{24b}$$

where ρ_I indicates the density of layer S_I and m_I the corresponding mass. Application of the lever rule to the underlying binary phase diagram (Figure 1) at temperature T_E affords the mass of the pure crystal of component 2, m_I, and the mass of the eutectic, m_{II}, as a function of the initial concentration of the sample, w_2°, and the composition of the eutectic point, w_2^E, in the mass fraction scale:[3]

$$m_I = m\frac{w_2^\circ - w_2^E}{w_2^s - w_2^E} \qquad m_{II} = m\frac{w_2^s - w_2^\circ}{w_2^s - w_2^E} \tag{25}$$

w_2^s herein denotes the concentration of the pure component of the respective equilibrium and is equated to zero or unity, respectively, depending on the initial composition w_2°. This means that $w_2^s = 0$ if $w_2^\circ < w_2^E$, and $w_2^s = 1$ if $w_2^\circ > w_2^E$.

The specific eutectic enthalpy of fusion, $\Delta\tilde{H}_{II}$, in eq 23 is furthermore determined by[3]

$$\Delta\tilde{H}_{II} = \frac{w_2^s - w_2^\circ}{w_2^s - w_2^E}[(1 - w_2^E)\Delta\tilde{H}_{01} + w_2^E\Delta\tilde{H}_{02} + \Delta\tilde{H}_{mix}^E] \tag{26}$$

where $\Delta\tilde{H}_{01}$ and $\Delta\tilde{H}_{02}$ are the specific enthalpies of fusion of the pure components 1 and 2, and $\Delta\tilde{H}_{mix}^E$ is the specific enthalpy of mixing at the eutectic composition w_2^E and the eutectic temperature T_E. It is worth noting that, owing to w_2^s = 0 or $w_2^s = 1$, eq 26 holds only for binary eutectic systems without any formation of mixed crystals. Otherwise, if $0 < w_2^s < 1$, eq 26 represents the specific eutectic enthalpy of a system showing a partial miscibility in the solid state.

As can be seen from eq 23, the eutectic enthalpy $\Delta\tilde{H}_{II}$, the resistances R_I and R_{II}, and the time t_0 depend on the intial concentration w_2°. Pursuant to eq 26 the eutectic enthalpy becomes maximum at $w_2^\circ = w_2^E$ and decreases linearly on either side of the eutectic point until the abcissa is intersected at $w_2^\circ = w_2^s$.[3,10,11] Correspondingly, ΔT_E in eq 23 should also have its maximum value at the eutectic point. Unlike resistance R_{II}, which decreases in the same manner since the portion of the eutectic crystal gets constantly smaller with rising distance from

the eutectic point, R_I and also t_0 are growing quantities, however, due to an increasing layer thickness Δz_I. It is thus conceivable that ΔT_E does not show a continuous course as a function of w_2° within $0 < w_2^\circ < w_2^E$ or $w_2^E < w_2^\circ < 1$. In other words, the eutectic peak widths might even reveal an additional (second) maximum width at $w_2^\circ \neq w_2^E$, as will be shown.

For this reason, we turn our attention to investigating the concentration-dependence of these peak widths in more detail. Since the eutectic point is usually shifted toward lower concentrations and quite frequently becomes identical with the melting point of the lower molecular component 1, first and foremost when using an oligomer as component 2 or rather a polymer (see, for instance, Figure 1), the following discussion is only performed for this latter case, $w_2^s = 1$. Equation 23 may hence be condensed to

$$\Delta T_E = \sqrt{C_3(1 - w_2^\circ)m\dot{T}_P(2R_0 + C_2m_I + C_1m_{II}) + (\dot{T}_P t_0)^2} \tag{27}$$

whereby C_1, C_2, and C_3 are defined by

$$C_1 \equiv \frac{1}{A^2\lambda_{II}\rho_{II}} = \frac{R_{II}}{m_{II}} \tag{28a}$$

$$C_2 \equiv \frac{2}{A^2\lambda_I\rho_I} = 2\frac{R_I}{m_I} \tag{28b}$$

$$C_3 \equiv \frac{1}{1 - w_2^E}[(1 - w_2^E)\Delta\tilde{H}_{01} + w_2^E\Delta\tilde{H}_{02} + \Delta\tilde{H}_{mix}] = \frac{\Delta\tilde{H}_{II}}{1 - w_2^\circ} \tag{28c}$$

By use of eq 17b and eq 25, differentiation of eq 27 with respect to the overall concentration, w_2°, yields

$$\left(\frac{\partial\Delta T_E}{\partial w_2^\circ}\right)_P = \frac{C_3m\dot{T}_P\left[-R_0 - \frac{1}{2}C_2m + m_{II}(C_2 - C_1)\right] + \dot{T}_P{}^2\left(\frac{\partial t_0}{\partial w_2^\circ}\right)_P}{\sqrt{C_3(1 - w_2^\circ)m\dot{T}_P(2R_0 + C_2m_I + C_1m_{II}) + (\dot{T}_P t_0)^2}} \tag{29a}$$

The second derivative is therefore

$$\left(\frac{\partial^2\Delta T_E}{\partial w_2^{\circ 2}}\right)_P = -\frac{\left[C_3m\dot{T}_P\left[-R_0 - \frac{1}{2}C_2m + m_{II}(C_2 - C_1)\right] + \dot{T}_P{}^2\left(\frac{\partial t_0}{\partial w_2^\circ}\right)_P\right]}{[C_3(1 - w_2^\circ)m\dot{T}_P(2R_0 + C_2m_I + C_1m_{II}) + (\dot{T}_P t_0)^2]^{3/2}} + \frac{-C_3m\dot{T}_P\frac{m}{1 - w_2^E}(C_2 - C_1) + \dot{T}_P{}^2\left(\frac{\partial^2 t_0}{\partial w_2^{\circ 2}}\right)_P}{[C_3(1 - w_2^\circ)m\dot{T}_P(2R_0 + C_2m_I + C_1m_{II}) + (\dot{T}_P t_0)^2]^{1/2}} \tag{29b}$$

As is apparent from eqs 29, the slope and curvature of the ΔT_E-(w_2°) curve are markedly governed by the difference $(C_2 - C_1)$ that also corresponds to the difference of the two resistances R_I and R_{II} related to the masses of their layers, m_I and m_{II}, respectively. Usually, however, C_1 and C_2 are of the same magnitude approximately, and the eutectic peak widths will hence decrease with growing composition w_2° (see eq 29a). Those terms containing the first or second derivative of t_0 with respect to w_2° are dominated by the other terms; they are thus negligible (error $\leq$ 1%).

Two limiting cases are hence to be discriminated; if $C_1 < C_2$, the $\Delta T_E(w_2^\circ)$ curve of eq 27 will be concave toward the w_2° axis, and the locus of the maximum eutectic peak width (i.e. the concentration at which the maximum eutectic peak width is found),

$$w_{2,max}^\circ = 1 - \frac{1 - w_2^E}{m(C_2 - C_1)}\left[R_0 + \frac{1}{2}C_2m - \frac{\dot{T}_P}{C_3m}\left(\frac{\partial t_0}{\partial w_2^\circ}\right)_P\right] \tag{30a}$$

derived by equating eq 29a to zero, will shift to negative concentrations, which are meaningless in physical terms. Only if

$$C_1 \leq \frac{1}{2}C_2 - \frac{R_0}{m} \tag{30b}$$

i.e. if C_2 exceeds C_1 by factor $(2mC_2)/(mC_2 - 2R_0)$, a maximum eutectic peak width will appear within the concentration range from w_2^E to unity ($w_2^E < w_{2,max}^\circ < 1$). On the other hand, if $C_1 > C_2$, $w_{2,max}^\circ \rightarrow +\infty$, and a maximum peak width will never occur at a concentration between w_2^E and 1 (see eq 30a). The $\Delta T_E(w_2^\circ)$ curve will also reveal a concave curvature as long as

$$C_1 < C_2 + \frac{C_3\dot{T}_P(1 - w_2^E)}{(\dot{T}_P t_0)^2}\left(R_0 + \frac{1}{2}mC_2\right)^2 \tag{30c}$$

Otherwise, the curve in question will turn to a convex curvature with respect to the w_2° axis, and eq 30a will represent the minimum peak width at a concentration that is, however, senseless in physical terms.

Let us conclude this section with a consideration of the heat flow recorded in the course of the eutectic transition and its proportionality to the specific heat capacity. To this end, we return to eq 20 again. Solving for z, and forming the first derivative from t, followed by incorporation into eq 18 yields

$$\dot{Q} = \frac{\dot{T}_P t}{R_0 + R_I} \times \sqrt{\frac{(m_I + m_{II})\Delta\tilde{H}_{II}\rho_{II}\lambda_{II}A^2(R_0 + R_I)^2}{m_I\dot{T}_P(t^2 - t_0^2) + (m_I + m_{II})\Delta\tilde{H}_{II}\rho_{II}\lambda_{II}A^2(R_0 + R_I)^2}} \tag{31}$$

For small values of t, eq 31 reduces to

$$\dot{Q}_{t \rightarrow t_0} \approx \frac{\dot{T}_P}{R_0 + R_I}\,t \tag{32}$$

This expression serves to determine resistance R_I or conductivity λ_I from the (average) slopes of the ascending branches of the experimental eutectic peaks, $(\partial\tilde{c}_P/\partial T)_P$, for instance, by linear regression; since the heat flow $\dot{Q}$ can be expressed as function of the specific heat capacity $\tilde{c}_P$,[12,13]

$$\dot{Q} = \tilde{c}_P m\dot{T}_P \tag{33a}$$

its first differential coefficient,

$$\left(\frac{\partial\dot{Q}}{\partial t}\right)_P = \left(\frac{\partial\tilde{c}_P}{\partial t}\right)_P m\dot{T}_P = \left(\frac{\partial\tilde{c}_P}{\partial T}\right)_P m\dot{T}_P{}^2 \tag{33b}$$

can be equated to the first derivative of eq 32,

$$\left(\frac{\partial \dot{Q}}{\partial t}\right)_P = \frac{\dot{T}_P}{R_0 + R_I} \tag{33c}$$

so that R_I can be established by the relation

$$R_I = \frac{1}{m\dot{T}_P\left(\frac{\partial \tilde{c}_P}{\partial T}\right)_P} - R_0 \tag{34}$$

Substituting eq 24a for R_I and eq 25 for m_I in eq 34, the reciprocal slopes,

$$\left(\frac{\partial \tilde{c}_P}{\partial T}\right)_P^{-1} = \beta + \alpha w_2^\circ \tag{35a}$$

prove to be a linear function of the initial concentration w_2° with the parameters

$$\alpha = \frac{1}{1 - w_2^E}\frac{m^2\dot{T}_P}{A^2\lambda_I\rho_I} \tag{35b}$$

$$\beta = m\dot{T}_P R_0 - w_2^E\frac{1}{1 - w_2^E}\frac{m^2\dot{T}_P}{A^2\lambda_I\rho_I} \tag{35c}$$

designating the slope and intercept of the line. Hence, plotting the reciprocal slopes of the ascending branches of the eutectic peaks against w_2° furnishes a straight line of which the slope α may be utilized to determine the thermal conductivity λ_I of layer S_I from eq 35b.

3. Experimental Section

3.1. Materials. Hydrocarbons used were *n*-eicosane (*n*-$C_{20}H_{42}$) and *n*-triacontane (*n*-$C_{30}H_{62}$) from Aldrich-Chemie, Steinheim, without further purification.

3.2. Thermal Analysis. Each sample whose average mass amounted to 1.58 mg (±0.07 mg) has been crystallized with a cooling rate of about 0.3 K·min^{-1}. Scans were carried out on a differential scanning calorimeter (DSC-2C) from Perkin-Elmer, combined with low-temperature equipment in a nitrogen atmosphere, with a scanning speed $\dot{T}_P$ of 10 K·min^{-1}. The eutectic temperatures, T_E, were evaluated as those corresponding to the right foot points of the peaks (peak ends). The shift of these temperatures versus heating rate has been considered by calibrating the temperature on the respective heating rate. Although the eutectic transition should be terminated at the maximum of the eutectic peak pursuant to eq 31, their widths ΔT_E have been taken from the total eutectic peak width, i.e. the descending branch inclusively, which corresponds to a systematic error in ΔT_E of about 1.0−1.5 K.

4. Results and Discussion

4.1. Eutectic Peak Widths. The thermal resistance R_0 was determined from DSC scans of pure components by application of eq 23. All quantities referred to the segment S_{II} have been assigned to the pure components, whereas resistance R_I and time t_0 have been equated to zero. Equation 23 hence reduced to an expression characterizing the peak width of a sharply melting substance. An expression equivalent to this but being somewhat different in form has been derived originally by O'Neill.[4] Analysis according to this simplified equation thus led to a thermal resistance R_0 of 57 K·s·J^{-1} on average. This quantity has been treated as a constant during the evaluation, although it was additionally found to be temperature dependent. In contrast to that, O'Neill arrived at a lower value of about 48 K·s·J^{-1} by use of a DSC-1.[4] This is clear inasmuch as in our experiments the total peak widths have been taken to comprise also the descending branches of the peaks.

The cross-sectional area A is, strictly speaking, not the area of the pan-holder.[4] In reality, A refers to the maximum diameter of the crystals. By taking the inner diameter of the aluminum-pans, we thus arrived at a value of 0.090−0.095 cm^2. Drawing a comparison to the sample-containers utilized by O'Neill,[4] of which the cross-sectional area amounts to 0.45 cm^2, implies that those are twice as large in diameter as our aluminum-pans. This also accounts for the discrepancy between our value for R_0 and that quoted by O'Neill (see eq 7).

The ascending branches of the eutectic peaks get flatter with growing concentration w_2° of *n*-triacontane (*n*-$C_{30}H_{62}$). In accordance with eq 35a, plotting the reciprocal slopes against w_2° yields a set of data points that may be fitted by linear regression to an ascending straight line with slope $\alpha = 1.344 \times 10^{-2}$ g·K^2·J^{-1}. Taking w_2^E to be 0.05 approximately (see Figure 1) and density ρ_I to be 0.80−0.81 g·cm^{-3},[14] we arrive at a value $\lambda_I = 46.86 \times 10^{-4}$ W·K^{-1}·cm^{-1}, which exceeds the literature value for solid normal-paraffins[14,15] by 84%! Owing to this unexpectedly large discrepancy in λ_I, the constants C_1 and C_2 have thus been established from literature data. Density ρ_{II} has been taken to be 0.76−0.77 g·cm^{-3};[15−17] the thermal conductivities amounted to $\lambda_I \approx (24-27) \times 10^{-4}$ W·K^{-1}·cm^{-1} and $\lambda_{II} \approx (10-15) \times 10^{-4}$ W·K^{-1}·cm^{-1}, whereby in the latter case λ_{II} has been estimated from literature data of similar organic liquids.[14,15] With these data at hand, we are capable of evaluating the signs of the slope and curvature of the $\Delta T_E(w_2^\circ)$ curve and—depending on the ratio of C_1 and C_2—the locus of the maximum width $w_{2,max}^\circ$ pursuant to eqs 30. For instance, since C_1 approximately amounts to 100−165 K·mW^{-1}·g^{-1} and $C_2 \approx$ 100−130 K·mW^{-1}·g^{-1}, we may assert that the eutectic peak widths will represent a constantly falling curve with concave curvature toward the concentration axis but without any maximum due to $C_1 > C_2$ that proceeds from $\lambda_{II}\rho_{II} < \lambda_I\rho_I$.

Yet the proper widths of the eutectic peaks are not predictable since eq 27 comprises a supplementary term, $(\dot{T}_P t_0)^2$, of which time t_0 cannot be determined due to the unknown temperatures T_{III} and T_P at time $t = t_0$. Furthermore, t_0 is conditional upon further quantities, such as the specific heat capacities of platform P (to be divided, strictly speaking, into the pan-holder and the aluminum-pan) and layer S_I, their respective masses, and the preset heating rate. It is, however, likely that time t_0 is subject to a relationship being similar to the expression for time t derived in eq 21. If $t_0 = \sqrt{a+bw_2^\circ}$ is taken, for instance, where a and b are parameters to be adjusted, ΔT_E may be fitted to the experimental data pursuant to eq 27. This is shown in Figure 4 by a solid line. The experimental data points designated by circles are additionally supplied with vertical bars representing the margin of error because the very beginning of the individual melting peaks cannot be specified mostly without a small uncertainty.

Inspection of the experimental data in Figure 4 confirms that the eutectic peak widths decrease as a function of w_2°. Due to the concave curvature of these experimental data points with respect to w_2° in Figure 4, C_1 will comply with the condition given by eq 30b. That is, C_1 will never exceed this limiting value of about 250 K·mW^{-1}·g^{-1}; otherwise a convex curvature would be observed. Recalling eq 27 and Figure 1, we may comprehend this behavior.

The eutectic enthalpy, $\Delta\tilde{H}_{II} = (1 - w_2^\circ)C_3$, and mass m_{II} of the eutectic melt (see eq 25) decrease from $w_2^\circ = w_2^E$ to $w_2^\circ = 1$, whereas mass m_I of the crystalline layer S_I increases (R_0 is considered to be unchanged). Since, as already set forth above, C_1 and C_2 are of the same magnitude, the second bracketed

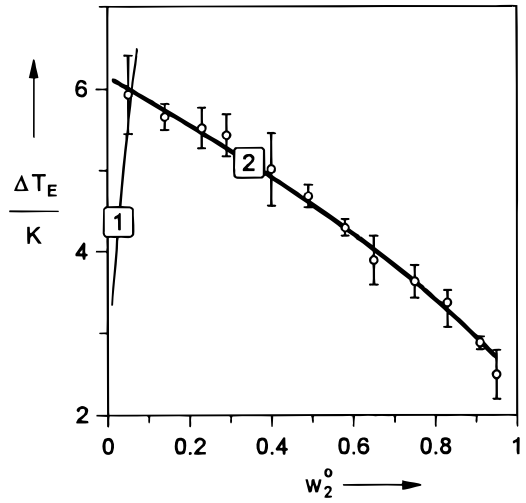

Figure 4. Concentration-dependence of the eutectic peak widths ΔT_E of n-$C_{20}H_{42}$/n-$C_{30}H_{62}$. ○: experimental data. Curves 1 and 2: calculated eutectic peak widths where $w_2^s < w_2^\circ < w_2^E$ and $w_2^s = 0$, or $w_2^E < w_2^\circ < w_2^s$ and $w_2^s = 1$, respectively, whereby curve 2 corresponds to the right-hand side equilibrium in Figure 1.

term in eq 27 remains unchanged on the whole throughout the entire concentration range. By multiplying this term by the eutectic enthalpy and the constant quantities m and $\dot{T}_P$, we obtain a term decreasing constantly and dominating the third bracketed term in eq 27, $(\dot{T}_P t_0)^2$, which eventually results in a continuously diminishing value of ΔT_E. Clearly, a maximum eutectic peak width will thus appear only if constant C_2 is noticeably larger than C_1 (i.e. $C_2 > C_1$) and the condition of eq 30b is met.

However, it should be observed that the appearance of a maximum ΔT_E and its locus, $w_{2,max}^\circ$, is somewhat under the control of the analyst (see eq 30b). For instance, the thermal resistance of the device, R_0, can be minimized by ensuring good thermal contact between the pan-holder and the sample-container being in contact with one another. Furthermore, the total mass of the sample, m, can be enhanced. Inasmuch as C_2 is conditional on the preparation of the sample, the occurrence of a maximum eutectic peak width at concentration $0 < w_{2,max}^\circ < 1$ will also be favored by a poorly crystallized layer S_I. That is, the more the density ρ_I is lowered, the larger C_2 (see eq 28b). Depending on the preparation of the test sample, constant C_2 and therefore the experimental peak width ΔT_E may vary, which might possibly fake a maximum width.

Drawing a comparison to our experimental data, the calculated eutectic peak widths ΔT_E turn out to be well-represented, at least, in a qualitative manner. Owing to the variation of the constants C_1 and C_2 that could be estimated only within certain ranges, times t_0 fitted to the experimental data are not particularly reliable. In our case, t_0 rises—depending on w_2°—from 10−20 s approximately. This means that temperature T_P at site z_P is raised within a period of t_0 by about 1.5−3 K with regard to the temperature T_I at interface z_I that has just arrived at the eutectic temperature T_E. In other words, at the beginning of the eutectic transition, i.e. when temperature T_I matches T_E at time t_0, temperature T_P exceeds T_E by the amount $\dot{T}_P t_0$.

4.2. Consideration of Errors. In this section, possible causes will be discussed from which the departure of our value from the literature value of thermal conductivity λ_I might arise. In doing so, we shall see that an exact determination of heat capacities by use of a dynamic calorimeter like DSC is in principle not possible. Finally, some consequences for the construction of state diagrams with a eutectic transition or an incongruently melting compound will be discussed.

First of all, a quite simple picture of a eutectic crystal, solidified in the aluminum-pan, has been adopted. According to Figure 3, the eutectic has been considered to be crystallized on top of crystal 2 precipitated before, whereby either crystal has further been regarded as a homogeneous and isotropic layer (S_I, S_{II}). In effect, however, the microstructure of the crystals forming is much more complex. Instead of uniform segments stated, there are, for instance, small crystallites, frequently enclosed in a matrix of the other crystal, that may entail surface phenomena. Furthermore, since n-paraffin crystals always have a sheetlike structure and are built up of regularly stacked layers,[18] the supposition of isotropic segments cannot really be maintained. In the end, crystallization and thus the microstructure of the forming crystals are also markedly governed by crystallization kinetics, such as the cooling rate, the number and stability of crystal nuclei, and their rate of formation and growth. For a more comprehensive picture of eutectic crystallization the reader is referred to textbooks of solid-state chemistry.[19,20]

Secondly, applying O'Neill's (already simplified) model for sharp melting transitions[4] to eutectic crystals, showing a sharp fusion as well, proves to be a further simplification. As it has been supposed by Brennan et al.,[21] melting does not proceed with a constant interfacial area A between the melt and the crystalline phases. Since this interfacial area will diminish during the fusion—at first very slowly but, as fusion progresses, faster and faster—the rate of fusion and therefore the enthalpy gradient $(\partial H_{II}/\partial t)_P$ will be reduced (see eqs 16 and 31). As a result, the rate of heat transfer at the end of the fusion process is lowered and the DSC curve is falling during the last portion of fusion, until the trace is coincidental with the heat capacity of the melt.[21] This, in turn, implies that the end of a fusion process—and thus the melting point—should be assigned to the end of a fusion peak and not to the temperature of its maximum value. From the same reason, ΔT_E has been determined from the total eutectic peak width (see section 3.2). It must be observed, however, that a conclusive judgement concerning the assignment of the melting temperature—either to the peak maximum or to the peak end—still remains elusive, as the explicit interrelation between the downward branch of a fusion peak and its underlying fusion process is not well understood yet. For practical purposes we prefer attributing the melting temperature to the peak end, which also results from the deconvolution of melting peaks of multicomponent systems.[22]

Thirdly, recalling eqs 33−35, we overlooked one crucial fact ("heat losses" of the measuring system caused by thermal radiations have not been taken into account inasmuch as these interferences are minimized by the twin device of the underlying calorimetric method (DSC[13]), or at least we disregarded it, which is, however, likely to account for most of the discrepancy between the thermal conductivity for n-eicosane (n-$C_{20}H_{42}$) quoted by Grigull and Sandner[14] and our value for λ_I established by linear regression from eq 35b. Pursuant to eq 33a, the heat flow, $\dot{Q}$, is correlated with $\tilde{c}_p$, where the heating rate $\dot{T}_P$ and the mass m of the sample are constants of proportionality. Here, $\tilde{c}_p$ is the overall heat capacity of the total sample at time t or temperature T, respectively. This involves both the enthalpy change due to a rise in temperature and that caused by fusion. Rate $\dot{T}_P$ is strictly speaking not the preset rate but, in fact, represents the mean value of temperature change of the total sample. Due to the fact that this quantity does not constitute a time average, the aforementioned heating rate must not necessarily remain constant during the DSC scan. In order to keep this (unknown) mean heating rate distinct from the (well-

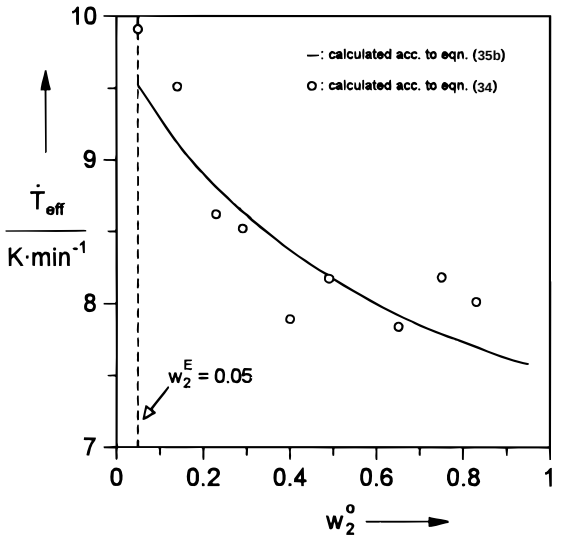

Figure 5. Effective heating rate ($\dot{T}_{eff}$) versus initial concentration calculated from eq 35b (—) and from eq 34 (○).

defined) preset heating rate $\dot{T}_P$ at site z_P, we substitute $\dot{T}_{eff}$, termed the effective rate, for $\dot{T}_P$ in eq 33a.

As we have seen above, any change of temperature at any site in the system is conditional on the thermal resistance of the layer involved and therefore depends on the respective layer thickness as well as its thermal conductivity (see eq 7). Consequently, $\dot{T}_{eff}$ is smaller, the larger the total resistance of the sample is. We may thus anticipate that substances with poor thermal conductive properties but also those with large overall masses lead to a diminution of this effective heating rate, regardless whether the test samples in question are subject to fusion or only to heating without undergoing a transition thereby. Hence, $\dot{T}_{eff} \leq \dot{T}_P$. Usually, the inequality holds. Only under certain circumstances, for instance when using metals as test samples, does the equality apply. In the event of the inequality, there is an additional time delay of heat conduction with respect to the elapsed time evaluated by eq 21, leading to a marginal distortion of the already smeared melting peak. This renders the ascending branches of the eutectic peaks a little steeper (see eq 34) owing to the diminished effective heating rate. Using $\dot{T}_P$ instead of $\dot{T}_{eff}$ in eq 34, the putative thermal resistance R_I will be lowered, yielding an enlarged value for the thermal resistance λ_I (see eq 24a).

On applying O'Neill's model[4] to eutectic fusion processes, an additional layer, S_I, of *n*-triacontane (*n*-$C_{30}H_{62}$) has been introduced, being a poor thermal conductor that is inert with regard to eutectic melting. As its layer thickness Δz_I increases with w_2^o pursuant to eqs 24 and 25, the effective heating rate $\dot{T}_{eff}$ must consequently decrease with growing initial concentration. Indeed, this is confirmed by the plot shown in Figure 5. Here, the overall effective rate, $\dot{T}_{eff}$, has been established from eq 34 after substituting $\dot{T}_{eff}$ for $\dot{T}_P$, and eq 24a for R_I, respectively, using the literature value for λ_I (circles). On the other hand, replacement of $\dot{T}_P$ with $\dot{T}_{eff}$ in eq 35b yielded the smoothed curve for $\dot{T}_{eff}$ (solid line) in Figure 5. Since $\Delta z_I = 0$ at $w_2^o = w_2^E$, the effective rate must be maximum at the eutectic point (here: at $w_2^E = 0.05$) and, accordingly, decrease again beyond this point toward lower concentrations, i.e. at $w_2^o < w_2^E$. We may thus conclude from eqs 35 that the reciprocal slopes plotted against the initial composition do not represent a straight line but, in fact, a curve getting slightly flatter with rising concentration. Hence, only the reciprocal slopes *additionally* related to the respective rate $\dot{T}_{eff}$ will increase linearly with w_2^o, as can be shown.

Furthermore, it should be observed that not only is the "proportionality" given by eq 33a affected by the total mass of the sample and the heat conductivity thereof it additionally depends on the preset rate $\dot{T}_P$. At increased heating rates, "heat losses" of the system are getting more and more apparent. These are irreversible processes like thermal radiations, being always a concomitant of heat conduction. Although the differential heat flow beween the test sample and the reference is registered in the DSC apparatus, the heat actually converted per unit time is smaller the larger the rate $\dot{T}_P$ is. This, in turn, renders the heat capacity $\tilde{c}_P$ of the DSC curve smaller.

Hence $\dot{T}_{eff}$ approaches $\dot{T}_P$ better the smaller the preset heating rate $\dot{T}_P$ and the mass of the sample and the larger the value of its thermal conductivity are, even if a pure substance is present. The exact applicability of eq 33a is therefore questionable, apart from metals as test samples. Judging from this point of view, exact calibration of specific heat capacities seems to be impossible.

Finally, let us point to a phenomenon associated with the construction of state diagrams with a eutectic transition. Inspection of Figure 1 reveals that the measured eutectic temperature T_E decreases with a growing initial concentration w_2^o. At the same time, Figure 1 further depicts a rise in the transition temperature T_T of the incongruently melting compound, $C_{30}H_{62}$. These two effects observed emerge from one and the same reason. Since mass m_{II} (eutectic) decreases and mass m_I (pure crystalline *n*-dodecane) proportionally increases to w_2^o pursuant to eq 25, the eutectic peak widths ΔT_E will constantly be diminished, as set forth above. Due to the calibration of the DSC, the peak widths and the specific enthalpies of fusion of the pure calibration samples approximately match those of the eutectic mixture at the eutectic point. Thus, the most trustworthy values of the eutectic temperature T_E should be found in the direct vicinity of the eutectic point. In other words, the more w_2^o differs from w_2^E, the more the eutectic temperature T_E is shifted toward lower temperatures, corresponding to an increasing deviation of the (experimentally faked) eutectic temperature from its proper (real) value. Moreover, smaller masses m_{II} will also result in smaller eutectic crystallites, which additionally brings about a decrease in the eutectic temperature of fusion, T_E, due to an increased surface−volume ratio of the crystal.[23−25] It is noteworthy, however, that although there is a rise in m_I in dependence of w_2^o such that the eutectic peak widths observed should broaden with rising w_2^o, the eutectic peak widths ΔT_E are still *not* yet of the same extent like that of the eutectic point (see Figure 4). That is, in spite of enlarged experimental ΔT_E values compared with those calculated, too low eutectic temperatures T_E will be found in fact.

For the same reason, state diagrams with an incongruently melting compound, as shown in Figure 1, represent a transition temperature T_T increase with growing w_2^o values. Here, the mass ratio of the melt and the remaining crystal consisting of the pure dodecane (component 2) will be changed in accordance with the lever rule. Consequently, diminishing the initial composition w_2^o renders the respective peak widths ΔT_T increasingly sharp owing to a decreasing mass of the pure solid component 2. This in turn results in transition temperatures that are lowered, indeed, originating an apparently decreasing course of the transition temperatures in question.

5. Conclusions

Owing to a finite thermal conductivity and a limited heat flow within the sample to be fused, the resulting melting peaks of pure compounds or eutectics turn out not to be infinitely sharp;

a time delay is observed instead leading to a peak broadening of a certain extent that is usually termed "smearing". This paper focused on investigating the concentration-dependence of the peak widths of the experimental, "smeared" eutectic fusion peaks. With this aim in view, O'Neill's model for sharply melting substances[4] has been modified, as depicted in Figure 3, by introducing an inert layer and applied to the eutectic fusion process. For the sake of a better comparability of these widths, the masses of the test samples were supposed to be as similar as possible.

Equation 23 derived proved itself to be suitable for a qualitative—or, at least, a semiquantitative—description of eutectic peak widths ΔT_E as a function of the initial composition w_2°. However, the accurate values of ΔT_E proved to be elusive inasmuch as the times t_0 are not known at all; here, time t_0 signifies the elapsed time until the eutectic transition commences. Furthermore, the individual thermal resistances could be estimated only within a certain range of reliability.

Pursuant to eqs 23−30, the eutectic peak widths in binary DSC diagrams have their maximum value at the eutectic point, i.e. at $w_2^\circ = w_2^E$, because at this locus, the eutectic enthalpy of fusion becomes maximum, too. Hence, the eutectic temperatures in isobaric phase diagrams established by DSC measurements will erroneously decrease with growing distance from the eutectic point (Figure 1). Under certain conditions, however, additional maxima in ΔT_E may appear, first and foremost, if the inert layer introduced (S_I) represents a quite poor thermal conductor, if the thermal resistance of the pan-holder (R_0) is diminished, or if the total mass of the test sample is increased (see eq 30b).

As it could be shown clearly from eq 33a, the correlation between the heat flow registered during a DSC scan and the specific heat capacity plotted against the temperature in DSC curves holds only if the preset heating rate $\dot{T}_P$ and the total mass m of the sample vanish whereas its thermal conductivity λ approaches infinity. Only in this particular event does the effective change of temperature in the sample remain constant and is almost equivalent to rate $\dot{T}_P$; at the same time, irreversible processes, such as "heat losses", are minimized. Otherwise a distortion of the resulting DSC melting peak with respect to time would become noticeable. We may thus conclude that a precise determination of heat capacities by means of DSC is questionable, except for systems with a high thermal conductivity like metals, for instance. This seems to be plausible inasmuch as DSC constitutes a dynamic measuring method while heat capacities refer to equilibrium states being slightly omitted in the course of a DSC performance.

Acknowledgment. The authors gratefully acknowledge financial support from the Deutsche Forschungsgemeinschaft (DFG). Thanks are also given to Dr. Ralf Jüschke for giving us permission to use his program "WinReg 8.92" for graphical representations.

References and Notes

(1) Ehrenfest, P. *Proc. Kon. Akad. Tetenschr. Amsterdam* **1933**, *36*, 153.
(2) Hemminger, W.; Höhne, G. *Calorimetry—Fundamentals and Practice*; Verlag Chemie: Weinheim, 1984; p 67ff.
(3) Müller, A.; Borchard, W. *J. Phys. Chem. B* **1997**, *101*, 4307.
(4) O'Neill, M. J. *Anal. Chem.* **1964**, *36*, 1238.
(5) Haase, R. *Thermodynamik der Mischphasen*; Springer: Berlin, 1956; p 561.
(6) Grigull, U.; Sandner, H. *Heat Conduction*, 2nd ed.; Springer: Berlin, 1990; p 7ff.
(7) Edwards, D. K.; Denny, V. E.; Mills, A. F. *Transfer Processes*; McGraw-Hill: New York, 1979; p 9ff.
(8) Eckert, E. R. G.; Drake, R. M. *Heat and Mass Transfer*, 2nd ed.; McGraw-Hill: New York, 1959; p 23ff.
(9) Jaeger, J. C.; Carlslaw, H. S. *Conduction of Heat in Solids*, 2nd ed.; Clarendon Press: Oxford, 1973.
(10) Tammann, G. *Z. Anorg. Chem.* **1903**, *37*, 303.
(11) Borchard, W.; Luft, B.; Reutner, P. *Ber. Bunsen-Ges. Phys. Chem.* **1984**, *88*, 1010.
(12) Dobnik, E. Ph.D. Thesis, Gerhard-Mercator-Universität Duisburg, Germany, 1991.
(13) Hemminger, W.; Höhne, G. *Calorimetry—Fundamentals and Practice*; Verlag Chemie: Weinheim, 1984; p 111.
(14) Grigull, U.; Sandner, H. *Heat Conduction*, 2nd ed.; Springer: Berlin, 1990; p 169ff.
(15) Weast, R. C., Ed. *Handbook of Chemistry and Physics*, 65th ed.; CRC Press: Boca Raton, FL, 1985.
(16) Sackmann, H.; Sauerwald, F. *Z. Phys. Chem.* **1950**, *195*, 295.
(17) Doolittle, A. K.; Peterson, R. H. *J. Am. Chem. Soc.* **1951**, *73*, 2145.
(18) Strobl, G. R.; Schwickert, H.; Trzebiatowski, T. *Ber. Bunsen-Ges Phys. Chem.* **1983**, *87*, 274.
(19) Kitaigorodsky, A. I. *Mixed Crystals*; Springer: Berlin, 1984; p 112ff.
(20) Rosenberger, F. *Fundamentals of Crystal Growth I*; Springer: Berlin, 1979; p 100ff.
(21) Brennan, W. P.; Miller, B.; Whitwell, J. C. *Ind. Eng. Chem. Fundam.* **1969**, *8*, 314.
(22) Kilian, H.-G. Private communication.
(23) Kilian, H.-G. *Koll. Z. Polym.* **1965**, *202*, 97.
(24) Kilian, H.-G. *Makromol. Chem.* **1970**, *139*, 115.
(25) Wunderlich, B. *Makromolecular Physics, Vol. 3: Crystal Melting*; Academic Press: New York, 1980; p 24ff.